PHILOSOPHICAL TRANSACTIONS OF THE ROYAL SOCIETY A MATHEMATICAL, PHYSICAL & ENGINEERING SCIENCES

Millimetre and Submillimetre Astronomy

P. E. Clegg, R. A. Newstead and J. A. Bastin

Phil. Trans. R. Soc. Lond. A 1969 **264**, 293-305
doi: 10.1098/rsta.1969.0027

Millimetre and submillimetre astronomy

By P. E. Clegg, R. A. Newstead and J. A. Bastin
Queen Mary College, University of London

[Plate 13]

Measurements of lunar radiation at a wavelength of 1·2 mm are described and discussed. It is found that the lunar poleward darkening function $T(\lambda\psi)/T(0\lambda)$ varies considerably more rapidly with latitude ψ than is predicted by a plane homogeneous model. Preliminary calculations using a centimetre scale roughness model are described. The results account well for the measured values of the darkening function at 1·2 mm as well as for measurements of the corresponding function at both longer and shorter wavelengths. Close to lunar dawn upland lunar areas appear to have higher brightness temperatures than the maria.

Some measurements of the partial solar eclipse of 20 May 1966 are reported together with observations of radiation from the planet Jupiter.

The relative advantages of Fourier transform and filter spectroscopy at millimetre and submillimetre wavelengths are discussed.

A possible experiment to detect the cosmic thermal 3 °K background at 1·3 and 1·9 mm wavelength is discussed.

It is the purpose of this paper to report briefly some observations of objects within the solar system made recently at Queen Mary College. The interpretation of these results will be discussed in some detail. The paper also considers the application of millimetre and submillimetre spectral techniques to astronomy and will end with the description of a possible experiment which could be used to detect the 3·2 °K thermal cosmic background radiation at 1·3 and 2·0 mm.

The dividing line between the microwave and infrared region is rarely a definite one but in astronomy there are technical reasons for setting it fairly clearly at about 2 mm. Above this wavelength narrow band superheterodyne receivers are used, and normal machine-engineering techniques are adequate for producing large radiation collectors. Below this wavelength wide-band bolometric techniques are mainly used while the most successful large radiation collectors are those whose profile has been produced by interference techniques with visual radiation. Finally above 2 mm, atmospheric absorption corrections are usually relatively small, whilst below this wavelength they can become the major source of error, and an observation has usually to be designed so that the effect of absorption on the final results is as small as possible.

Although this is the only paper presented at this meeting which deals with measurements in the 1–2 mm wavelength range, we wish to stress that this paper is in no way intended as a review of observations in this range. Important results have already been reported both by Low (1965, 1966), Low & Davidson (1965) and by Fedoseev (1963).

1. Instrumentation

The observations were made by means of an indium antimonide cooled photoconductive detector. This is a development of the type first described by Kinch & Rollin (1963) and is operated in zero magnetic field; impedance matching to the input of the pre-amplifier is by means of a 100:1 turns ratio cooled step-up transformer.

The detector is mounted on the 1·5 m $f/2{\cdot}2$ Cassegrain telescope installed at Queen Mary College. Convergent radiation from the secondary mirror is mechanically square wave modulated at the focus, passes through an inverted cone at the top of the light pipe and is condensed onto the crystal at the bottom of the pipe. Two choppers are used. For the normal measurements the chopper is a disk containing twenty holes around the circumference. For the detection of polarized radiation the chopper consists of a disk with forty holes around the circumferences containing alternate orthogonally oriented polarizers, with an inner ring of twenty holes for the phasing signal. This polarizing chopper measures directly the difference between radiation polarized in two orthogonal directions (Carter & Clegg). The modulating frequency is 1 kHz and the secondary of the step-up transformer is tuned to this frequency. (See figure 11, plate 13.)

The signal from the transformer is fed to a transistorized preamplifier and amplifier employing field effect transistors which has been developed in the laboratory. Thence the signal passes to a transistorized phase-sensitive detector of the type discussed by Williams (1965). The phasing signal is provided by a light beam, modulated by the chopper, falling on a photocell and phasing is mechanical. The signal from the phase-sensitive detector can be fed either to a pen recorder or to the Enhancetron unit which is described below.

In order to increase the signal/noise ratio for weak signals such as those from planets and the degree of polarization of lunar radiation, it is necessary to sum a large number of signals. Furthermore, in view of the non-white character of atmospheric noise (Park & Clegg) it is desirable that each signal should be obtained in as short a time as possible. For this reason the conventional drift-scan technique was rejected and the following automatic method of summing signals was devised.

The source was tracked continuously in hour angle by visual monitoring, and the telescope was nodded in declination about the mean position of the source. The total variation in declination could be varied between 30 min arc and 1° 30′ arc to suit the source.

The signal from the phase-sensitive detector was integrated for about 0·5 s. Since the radiation reaching the detector from any extraterrestrial source is only a small fraction of the background radiation from the atmosphere it was necessary to remove the d.c. level associated with this atmospheric radiation by applying a d.c. bias. The signal was then fed to the Nuclear Data Corporation 'Enhancetron' which consists of an analogue-digital converter, a 1024 location magnetic core store with an address scanning time base. This time base could be adjusted to suit the rate of declination drive of the telescope. In this way each declination scan across the source could be stored as a series of 1024 numbers. Successive scans could be added to those already stored, and the whole processes was made automatic by feeding the Enhancetron with a triggering pulse taken from the declination drive mechanism. The maximum rate of collecting data was about 1·3 scans/min so that

by observing for an hour an increase in signal/noise ratio of about 10 could be obtained. The sum of these scans could then be converted into analogue form by reading out the contents of the store onto a pen recorder at any desired rate. (See figure 12, plate 13.)

2. Observations and their interpretation

Lunar measurements

A number of brightness temperature measurements over the whole lunar disk nave recently been made at various lunar phases. It is hoped to report these in detail in a later publication, but for the present discussion we shall confine our attention to a single set of measurements made on 21 February 1967, 2 days before full moon.

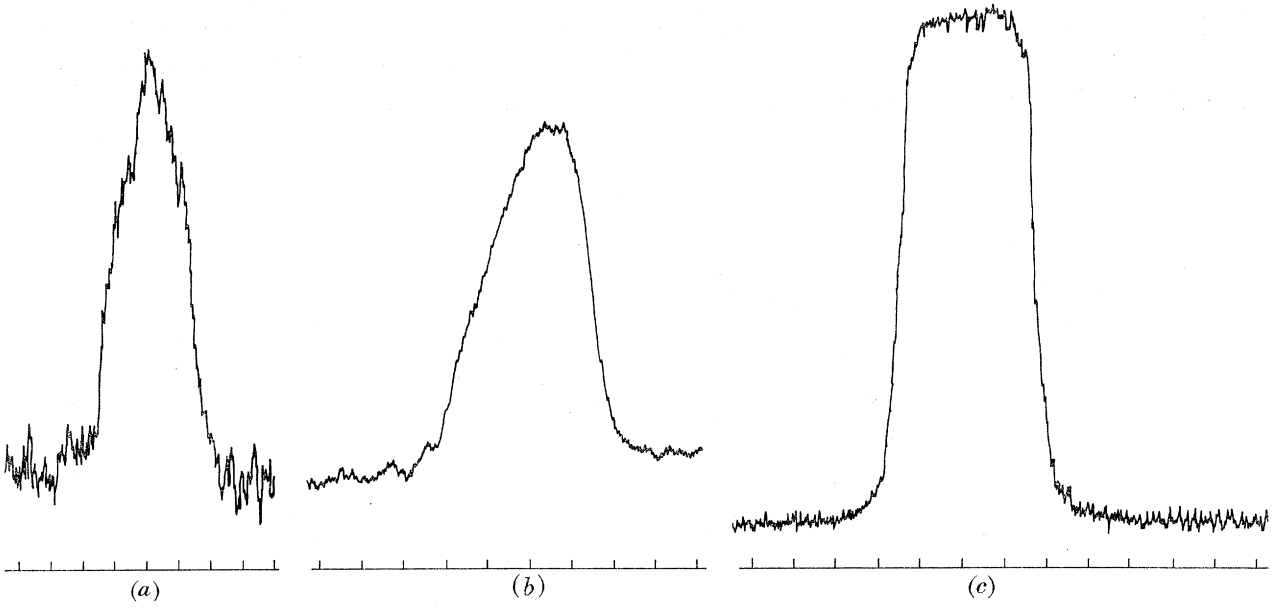

Figure 1. Lunar and solar scans at 1·2 mm wavelength. (*a*) Lunar scan in declination: scan line 1′ east of lunar meridian: lunar phase angle 325° (21. ii. 67) resolution half width 5′; (*b*) lunar scan in hour angle along equator: lunar phase angle 295° (29. iv. 66) resolution half width 9′; (*c*) solar equatorial scan (26. iv. 66) resolution half width 5′. In each case the interval between consecutive horizontal divisions corresponds to an angle of 10′.

The measuring technique employed was similar to that already reported (Bastin & Gear 1967) except that scans were made in a declination, rather than hour-angle, direction. The angular resolution, signal/noise ratio and pointing accuracy were also considerably improved. A typical scan is shown in figure 1, together with equatorial scans of both the Sun and Moon. Scans were made at an interval of 3·4′ in hour-angle and the intensities were plotted on a map of the lunar disk. The edge restoration technique invented by Gary (Gary, Stacey & Drake 1965) was then used to correct for the effect of the finite beam width of the telescope. The edge restoration function was calculated from solar equatorial drift curves, assuming that the solar source function at these wavelengths is a double step function of width equal to the visual width. Calculations for both millimetre (Coates 1958) and submillimetre wavelengths (Lena 1966) suggest that this is a sufficiently good approxi-

mation for the necessary corrections which are in any case small over the greater part of the lunar disk.

The intensities were converted to brightness temperatures assuming the Rayleigh–Jeans form of Planck's law. The normalization factor was determined by assuming the usual theoretical expression at the subsolar point, for the brightness temperature T at wavelength λ:

$$T = (1-R(\xi)) \sum_{n=0}^{\infty} \frac{T_n}{(1+2\delta_{n\xi}+2\delta_{n\xi}^2)^{\frac{1}{2}}} \cos(\epsilon_n - \phi_n), \tag{1}$$

where $\tan\phi_{n\zeta} = \delta_{n\zeta}/(1+\delta_{n\zeta})$, $\delta_{n\zeta} = \delta n^{\frac{1}{2}}(1+\sin^2\zeta/\epsilon)^{\frac{1}{2}}$ and $\delta = \beta/k_\lambda$. In these expressions ξ is the zenith angle, and $R(\xi)$ is the reflexion coefficient at the subsolar point, δ is the ratio of the absorption coefficient of the first harmonic of the synodic thermal wave to the electromagnetic absorption coefficient k_λ, T_n and ϵ_n are respectively the coefficients and phase angles resulting from a harmonic analysis of the temperature wave at the surface and ϵ is the dielectric constant for lunar rock. Equation (1) follows from the more general expression for the lunar microwave temperature (Bastin *et al.* 1964*b*).

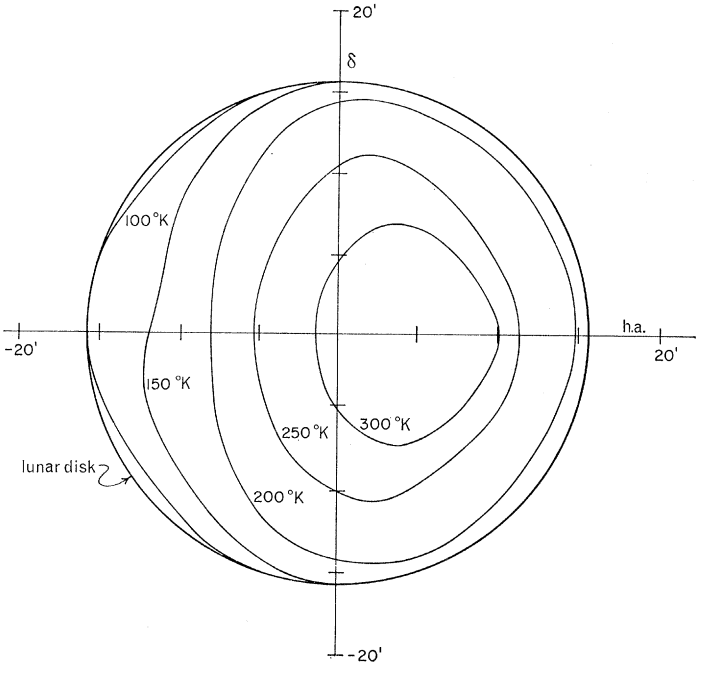

FIGURE 2. Lunar brightness temperature contours at 1·2 mm., lunar phase angle 325° (21. ii. 67).

In deducing a subsolar temperature from this equation a value of $\epsilon = 2$ has been assumed whilst the values of T_n and ϵ_n are those given by Sinton (1962). A value of $\delta = 0{\cdot}30$ was assumed and this was deduced from an interpolated mean of eclipse and lunation results reviewed by Bastin & Gear (1967). These values used with (1) give a subsolar brightness temperature of 325 °K, and the measured intensities were then normalized so that the subsolar point has this temperature. Contours at 50° intervals were then interpolated and the results are shown in figure 2.

The mean effective wavelength of the observations was found to be 1·15 mm with a mean spread of 0·25 mm. Both the mean and the spread were calculated from radio-sonde measurements made 30 miles away at Crawley by using the experimental values for the absorption coefficient (see for example Bastin 1966). From these calculations it seems likely that some 20 % of the radiation was located in the submillimetre window centred at 860 μm and further 10 % in the 740 μm window.

In the past (Bastin *et al.* 1964*b*) we have reported a number of contour maps of the lunar surface and noted that the lunar contours were apparently elongated in the equatorial direction considerably more than would be expected from the theory of a homogeneous moon with a plane parallel surface. We have attributed the cause of this discrepancy to centimetre-scale roughness of the lunar surface, without giving any detailed analysis of the process.

Now, however, that the present results have been established with considerably greater accuracy we have attempted an analysis of the thermal flow properties of a rough surface. Some of the results will be presented here, although it is hoped to present a more comprehensive account of the work at a later stage.

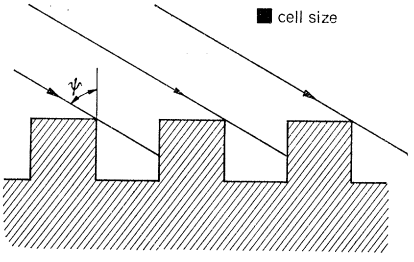

FIGURE 3. Centimetre-scale roughness model for the lunar surface.

We shall consider the roughness model shown in figure 3. The cooling of models of this type during an eclipse have already been treated by Winter (1965) and Bastin (1965). Here we consider the approach to equilibrium of the indented model for points on the lunar surface lying on the meridian which contains the subsolar point. We imagine the model orientated so that the normals to all the surfaces and the direction of the incident solar radiation are coplanar: the problem thus reduces to a two-dimensional thermal flow calculation. To reduce the number of variables to manageable proportions we have assumed the following values: lunar rock density, 1 g cm^{-3}; lunar specific heat, 0·2 cal g^{-1}; lunar rock thermal conductivity, 10^{-5} cal cm^{-1} °K^{-1}; horizontal indentation interval, 8 cm; indentation depth, 4 cm. The thermal flow was calculated by dividing the whole model into cubical cells 1 cm^3 in volume whose temperature was assumed to remain constant for a short interval of time t' during which the heat conducted and radiated to and from the cell was determined. The resulting change of temperature of the cell was then calculated, and the process repeated. Some of the results so far obtained are shown in figures 4 and 5, for two values of the lunar ψ. The depth of the indentations is considerably less than the penetration depth d, of the first harmonic (or period P) of the temperature wave during a lunation:

$$d = PK/\rho c.$$

It was thus to be expected (and this was in fact found to be the case) that the temperature of a layer well below the indentations assumed a value which tended to constant in a time several orders less than P. We can thus determine these mean subindentation temperatures for a number of lunar latitudes and phase angles and solve the thermal flow problem below this depth in the normal manner [see, for example, Wesselink (1948) and Jaeger (1953)].

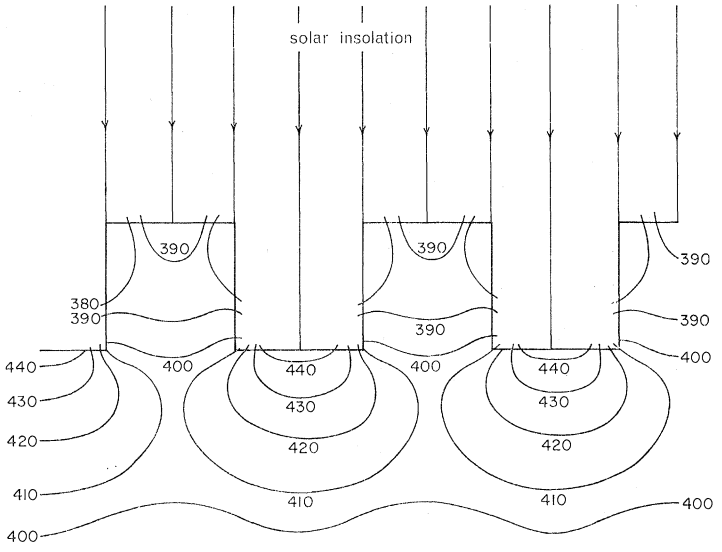

FIGURE 4. Temperature distribution at latitude 0° for a centimetre-scale lunar roughness model after 40 relaxation stages. An initial temperature of 396 °K was assumed in agreement with the equilibrium plane homogeneous model.

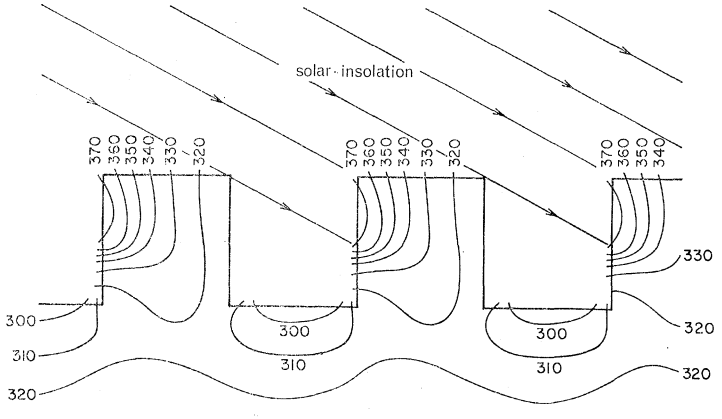

FIGURE 5. Temperature distribution at latitude 63·5° for a centimetre-scale lunar roughness model after 40 relaxation stages. An initial temperature of 326 °K was assumed in agreement with the equilibrium plane homogeneous model.

We shall restrict our discussion to points on the lunar meridian containing the subsolar point. For these points using the analysis of Krotikov & Shchuko (1963) or Gear (1965) we obtain for the brightness temperature $T(\psi\lambda)$ for a smooth plane parallel homogenous model:

$$T(\psi\lambda) = [1-R(\xi)] \sum_{n=0}^{\infty} \frac{T_n \cos^{\alpha_n}\psi}{(1+2\delta_{n\zeta}+2\delta_{n\zeta}^2)^{\frac{1}{2}}} \cos(\epsilon_n - \phi_n) \qquad (2)$$

where α_n takes the values 0·20, 0·33, 0·27 and 0·44 for the zero, first, second and third harmonics. From this expression the poleward lunar limb darkening function:

$$\eta(\psi\lambda) = T(\psi\lambda)/T(0\lambda) \tag{3}$$

may readily be calculated. It is found that for the variation of $T(\psi\lambda)$ given by (2) and also for *measured* values of the surface temperature and microwave (subsurface) temperatures the darkening expression approximates accurately to

$$\eta(\psi\lambda) = T(\psi\lambda)/T(0\lambda) = \cos^{m_\lambda}\phi, \tag{4}$$

where m_λ is a constant whose introduction does not introduce appreciable error but reduces the number of variables in the comparison. The measured values of m_λ do not agree with those calculated from equation (2) (plane homogeneous model) either in the

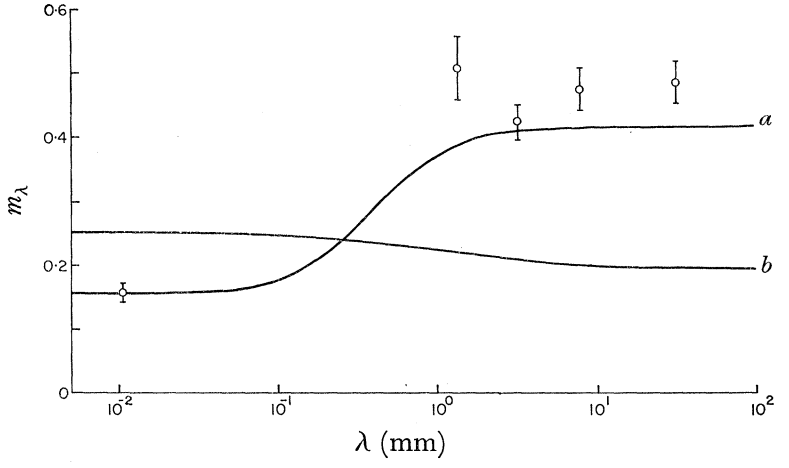

FIGURE 6. The poleward lunar limb darkening function along the meridian at full moon. The continuous curves are theoretical predictions for two models: *a*, Rough (indented) model; *b*, plane homogeneous model. The experimental points, in order of increasing wavelength follow respectively from the results of (i) Saari & Shorthill (1965), (ii) work described in this paper, (iii) Gary *et al.* (1965), (iv) and (v) Salomonovich (1962, 1967).

infrared (surface) or microwave (subsurface) case. The results are shown graphically in figure 6. The theoretical value of m_λ is plotted as a function of λ for both the plane homogeneous model and the indented model discussed above. The value of δ was assumed related to λ by the expression

$$\delta = 2{\cdot}2\lambda \text{ cm}^{-1}, \tag{5}$$

an expression which may deduced from both eclipse and lunation data over a considerable wavelength range (see Troitsky 1967; Bastin & Gear 1967).

For the smooth model, the value of $T(\psi\lambda)$ and hence m_λ was computed from (2). For the indented model the value of $T(\psi\lambda)$ was found by using temperature distribution of the model for various values of ψ two of which are shown in figures 4 and 5. The electromagnetic absorption coefficient for lunar rock was deduced from the expression:

$$\kappa_\lambda = \omega\rho c/2k^2\delta^2 \tag{6}$$

and the attenuation of the thermal emission from the individual surface and subsurface elements was thus computed. It is seen that the plane homogeneous model agrees poorly with observation while the indented model accounts reasonably well for the results of observations of both the infrared and microwave lunar thermal radiation. Rough calculations show that the difference to be expected between the brightness temperatures for the rough and smooth models increases approximately linearly with the depth/interval ratio of the indentations. Since for the indented model considered here this ratio is 0·5 we may conclude by extrapolation that the polar limb darkening properties of the thermal emission of the Moon may be explained by assuming the surface to be covered by indentations of area equal to the raised portions, and having a depth/interval ratio of about 0·7. To test whether or not this hypothesis is correct it would of course be very useful to make measurements in the 360 μm window to see if the value of m_λ has the predicted value.

In defence of this present hypothesis we add in conclusion the following considerations:

(1) The centimetre-scale roughness hypothesis has been successfully employed to explain (at least on a qualitative basis) a number of other features of the Moon's thermal radiation properties.

(2) Although the conductivity of lunar rock almost certainly increases with temperature (Muncey 1958; Clegg *et al.* 1966) such an increase with a plane parallel model cannot account for infrared values of $m_\lambda < \frac{1}{4}$, but rather produces the reverse effect. The increase of conductivity with depth (Jaeger 1953) is equally unable to account for the effect. Decrease of conductivity with increase of either temperature or depth seems physically unlikely, as does any systematic structural change of the properties of lunar rock with latitude.

In addition to the above results the declination scans across the lunar disk show in many cases a skew symmetry. This effect, which is particularly noticeable for the scans around lunar dawn, indicate a *lower* brightness temperature for the lunar highland regions than for maria. Similar results were found by Salomonovich (1967) at 8 mm.

Solar eclipse measurements

Seventeen scans at constant solar latitude or longitude were made across the Sun–Moon system during the partial solar eclipse of 20 May 1966. A typical scan is shown in figure 7. From an analysis of this and two other scans the mean disk temperature is found to have a value $1{\cdot}11 \pm 0{\cdot}03$ of that of the central temperature thus indicating solar limb brightening (see also Newstead 1968).

Radiation from the planet Jupiter

Figure 8 shows the sum of 153 drift curves across Jupiter. The signal/noise ratio obtained in these experiments is perhaps a factor of 30 poorer than obtained by Low (1966). Of this the greatest factor ($\sim$ 10) is due to the greater collecting area of the 200 in. Mount Palomar telescope. Other factors of the order of 2 may be introduced by lower atmospheric attenuation at Mount Palomar, by the more efficient optics of the Mount Palomar instrument, and possibly, by the sensitivity ratio of the detectors used.

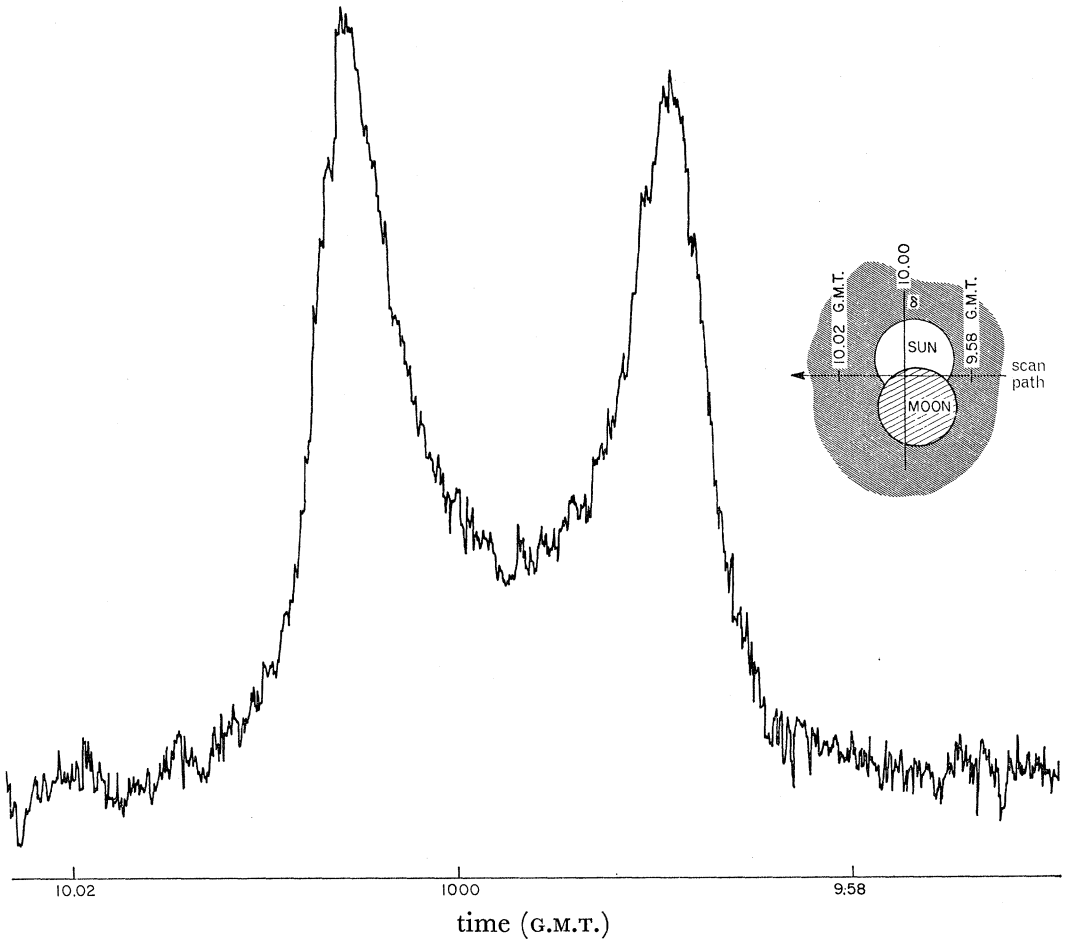

FIGURE 7. Drift curve scan during the solar eclipse of 20 May 1966. The inset shows the approximate path of the direction of the axis of the telescope during the scan.

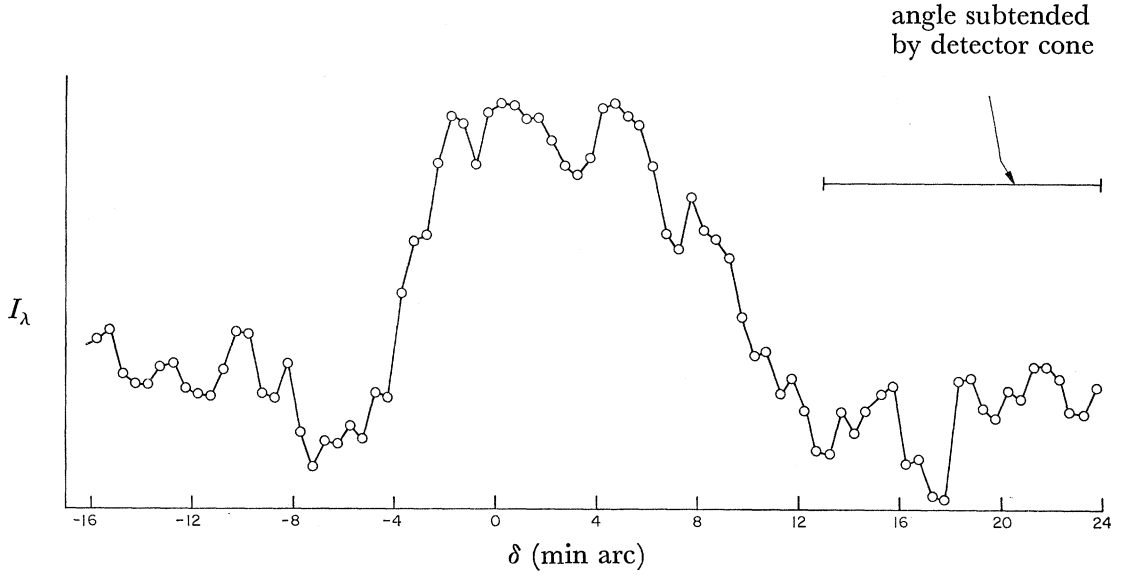

FIGURE 8. Sum of 153 scans of the planet Jupiter obtained on the nights 22. xi. 66, 3. xii. 66, 4. ii. 67 and 17. ii. 67. All the scans recorded on any given night were automatically summed by the technique described in the text.

3. Spectral techniques

In this section we compare the relative advantages of transform spectroscopy and the use of filters for astronomical measurements in the far-infrared.

(*a*) *Fourier transform spectroscopy*

The ability of the Fourier transform method to produce high resolution spectra in the millimetre and submillimetre region has been very successfully demonstrated by Gebbie (1957, 1958) and this work has been repeated more recently by other workers (e.g. Williams & Chang 1966). By using high altitude sites ($\sim$ 3 km elevation) the method in effect at present only produces a water-vapour spectrum using the Sun as a source. However, the method has clearly high potentiality and with little adaptation should be applicable to the search for molecular and molecular-radical pure-rotational transitions in the solar spectrum. For this purpose the telescope would ideally be mounted on a high flying aircraft or balloon at between 15 and 20 km elevation. Below this height the presence of water-vapour and oxygen absorption lines would make the interpretation of solar spectra difficult although not impossible. In addition, at these lower altitudes, noise due to variations in the brightness temperature of the terrestrial atmosphere may make the system less efficient than a conventional spectrometer.

The spatial analogue of the transform spectrometer would seem to be well worth applying to millimetre and submillimetre astronomy. For example, by this method the information required for the contour map shown in figure 2 could all be obtained from a single scan.

(*b*) *Fabry–Pérot etalons and interferometers*

The use of the Fabry–Pérot interferometer for astronomical measurements in the millimetre and submillimetre range has been described by Gaitskell & Gear (1966). It is difficult to construct such an interferometer with a wavelength resolution which approaches the resolution that can be obtained using transform spectroscopy. However, a Fabry–Pérot filter can be readily constructed so that it passes most of the radiation transmitted by any given atmospheric window in the range 200 to 2000 μm, and very little of the radiation transmitted by any of the other windows. In this way the photometric system of lettered spectral ranges with associated filters, extended to the mid-infrared by Johnson and others (Johnson 1965; Johnson *et al.* 1966) may now be further extended to include far-infrared work. For filters of this type, having a Lorentzian transmission characteristic and half width $\Delta\lambda \approx 0{\cdot}1\,\lambda$, we therefore suggest the following terminology in which the figures in brackets represent in each case the wavelength of the transmission maximum: S (360 μm), T (460 μm), W (740 μm), X (860 μm), Y (1360 μm) and Z (1900 μm).

Possibility of the detection of the cosmic thermal background at wavelengths 1·3 *and* 1·9 mm

Previous determinations of the cosmic thermal background (Penzias & Wilson 1965; Roll & Wilkinson 1966) have all been carried out in the wavelength range above 2 cm. Above this wavelength a blackbody at 3·2 °K emits only 0·1 % of its total radiative energy. However, at about 1·5 mm the spectral energy I_ν reaches a maximum. In fact, if

we assume that this radiation pervades extragalactic as well as intergalactic space then we arrive at the conclusion that 80 % of the *total* radiation in the universe is located within an octave of 1·5 mm, a fact which may perhaps be cited in favour of the development of astronomy at these wavelengths. Although recent experiments (Thaddeus & Clausser 1966) in the visual wavelength region infer that the radiation has still a 3 °K brightness temperature at 3 mm, it seems desirable to have a more direct check, if possible at a wavelength which is centred even closer to the peak of the blackbody distribution. Some cosmological models (Weymann 1966) in fact predict a cosmic radiative spectrum which is markedly non-Planckian at about 1 mm wavelength.

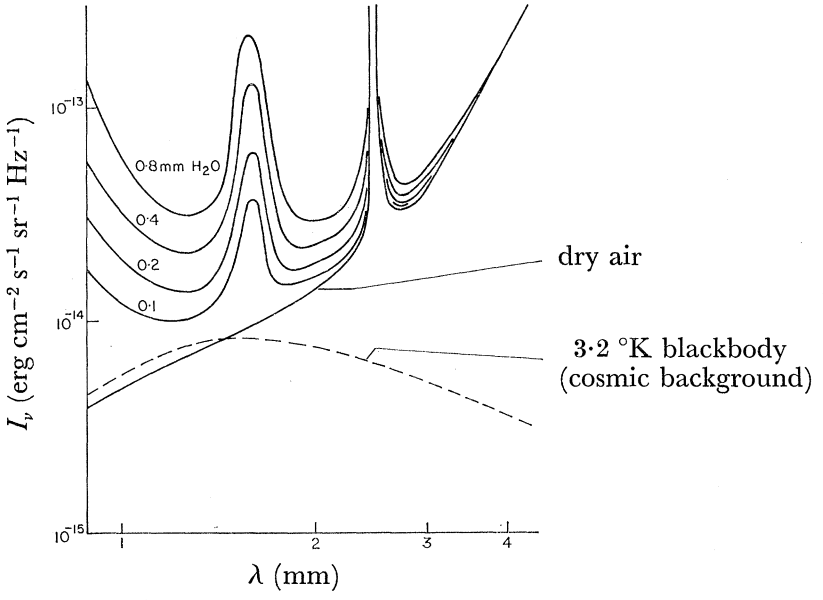

FIGURE 9. Cosmic background and atmospheric radiation for various water-vapour concentrations. Because of the somewhat uncertain extrapolation the pressure induced nitrogen and oxygen absorption reported by Heastie & Martin (1962) has not been included in the calculations.

Figure 9 shows the radiation to be expected from the cosmic background and also from an atmosphere at sea-level with various water-vapour concentrations. It is seen that at the wavelengths 1·3 and 1·9 mm the atmospheric radiation does not exceed the cosmic background by more than a factor of about 2. It should therefore be possible to eliminate the effect of the atmospheric radiation by making measurements at various zenith angles. The system could be calibrated with blackbody cavities kept at 77, 273, and 373 °K with liquid nitrogen, ice and steam. A possible experimental arrangement is shown in figure 10. The entrance cone, *A*, gives considerable directivity to the radiation passing through the modulator, *B*. The radiation then passes through an inverted cone *C* which decreases its mean acceptance angle so that it crosses the etalon filter, *D*, almost normally and is then refocused onto a cooled detector *E*. It should be stressed that the experiment requires either very high altitudes or very cold sites (Gaitskell, Newstead & Bastin, this volume, p. 195). The former have the advantage that the oxygen emission has a linear dependence (per molecule) on pressure, so that, for example, at about 4·5 km the oxygen absorption

has dropped to about half its sea-level value. Very cold sites on a level terrain would have the advantage that the atmosphere above them probably obeys the plane parallel approximation reasonably well so that the elimination of the effect of atmospheric radiation would be more exact. The Amundsen–Scott base at the South Pole would probably be an ideal site for the experiment.

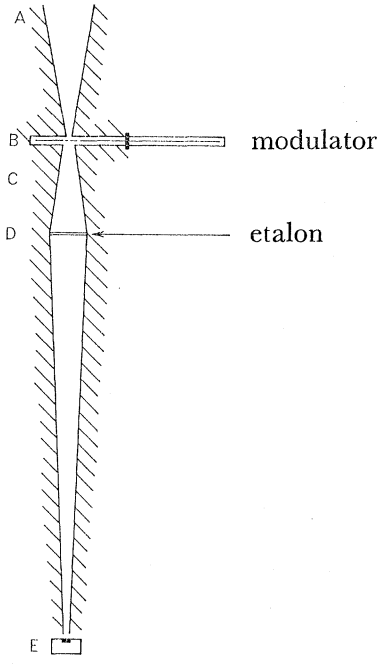

FIGURE 10. Instrumental arrangement for a possible cosmic background experiment at 1·3 and 1·9 mm.

We are indebted to Mr A. C. Marston and Mr D. G. Vickers for invaluable help and advice in the design construction and operation of the equipment and to Mr T. W. Pritchard for his work in designing the associated electronic circuitry.

We wish to thank the Science Research Council and Professor G. O. Jones for a great deal of support.

REFERENCES (Clegg *et al.*)

Bastin, J. A. 1965 *Nature, Lond.* **207**, 1381.
Bastin, J. A. 1966 *Infrared Phys.* **6**, 209.
Bastin, J. A., Clegg, P. E., Gear, A. E., Jones, G. O. & Platt, C. M. 1964*b* *Nature, Lond.* **203**, 960.
Bastin, J. A. & Gear, A. E. 1967 *Proc. Roy. Soc.* A **296**, 348.
Bastin, J. A., Gear, A. E., Jones, G. O., Smith, H. J. T. & Wright, P. J. 1964*a* *Proc. Roy. Soc.* A **278**, 543.
Carter, B. S. & Clegg, P. E. (In preparation.)
Clegg, P. E., Bastin, J. A. & Gear, A. E. 1966 *Mon. Not. R. Astr. Soc.* **133**, 63.
Coates, R. J. 1958 *Astrophys. J.* **128**, 83.
Fedoseev, L. N. 1963 *Radiofiz* **6**, 655.
Gaitskell, J. N. & Gear, A. E. 1966 *Icarus* **5**, 237.
Gary, B., Stacey, J. & Drake, F. D. 1965 *Astrophys. J.* Suppl. no. 108.

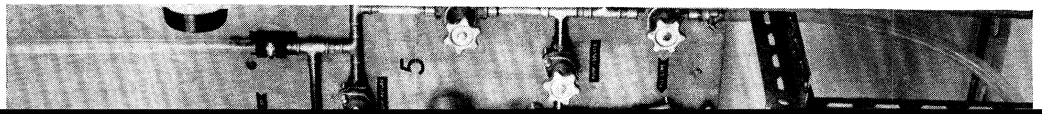

(1)
(3)
and

PHILOSOPHICAL TRANSACTIONS OF THE ROYAL SOCIETY A MATHEMATICAL, PHYSICAL & ENGINEERING SCIENCES

Gear, A. E. 1965 Thesis, London University.
Gebbie, H. A. 1957 *Phys. Rev.* **107**, 1194.
Gebbie, H. A. 1958 *J. Phys. Radium* **19**, 230.
Heastie, R. & Martin, D. H. 1962 *Canad. J. Phys.* **40**, 122.
Jaeger, J. C. 1953 *Aust. J. Phys.* **6**, 10.
Johnson, H. L. 1965 *Astrophys. J.* **141**, 170.
Johnson, H. L., Mitchell, R. I., Iriarte, B. & Wisniewski, W. Z. 1966 *Comm. Lunar and Planetary Laboratory, Univ. Ariz. Tucson* **4**, 99.
Kinch, M. A. & Rollin, B. V. 1963 *Br. J. Appl. Phy.* **14**, 672.
Krotikov, V. D. & Shchuko, O. B. 1963 *Sov. Ast.* **7**, 228.
Lena, P. 1966 *Annales Astrophys.* **29**, 361.
Low, F. J. 1965 *Astrophys. J.* **142**, 1287.
Low, F. J. 1966 *Proc. I.E.E.E.* **54**, 477.
Low, F. J. & Davidson, A. W. 1965 *Astrophys. J.* **142**, 1278.
Muncey, R. W. 1958 *Nature, Lond.* **181**, 1459.
Newstead, R. A. 1968 *Solar Physics* (in the press).
Park, W. McN. & Clegg, P. E. (In preparation.)
Penzias, A. A. & Wilson, R. W. 1965 *Astrophys. J.* **142**, 419.
Roll, P. G. & Wilkinson, D. T. 1966 *Phys. Rev. Lett.* **16**, 405.
Saari, J. M. & Shorthill, R. W. 1966 Boeing Sci. Res. Lab. Rep. D 1-82-0586. Seattle.
Salomonovich, A. E. 1962 *Sov. Astron.* **6**, 55.
Salomonovich, A. E. 1967 *Proc. Roy. Soc.* A **296**, 354.
Sinton, W. M. 1962 *Physics and astronomy of the Moon* (ed. Z Kopal), chap. XI. New York and London: Academic Press.
Thaddeus, P. & Clauser, J. F. 1966 *Phys. Rev. Lett.* **16**, 819.
Troitsky, V. S. 1967 *Proc. Roy. Soc.* A **296**, 366.
Wesselink, A. J. 1948 *Bull. Astr. Insts. Netherlds.* **10**, 351.
Weymann, R. 1966 *Astrophys. J.* **145**, 560.
Williams, P. 1965 *J. Sci. Instrumen.* **42**, 474.
Williams, R. A. & Chang, W. S. C. 1966 *Proc. I.E.E.E.* **54**, 462.
Winter, D. F. 1965 Boeing Sci. Res. Lab. Rep. D 1-82-0449.

PHILOSOPHICAL TRANSACTIONS OF THE ROYAL SOCIETY A MATHEMATICAL, PHYSICAL & ENGINEERING SCIENCES

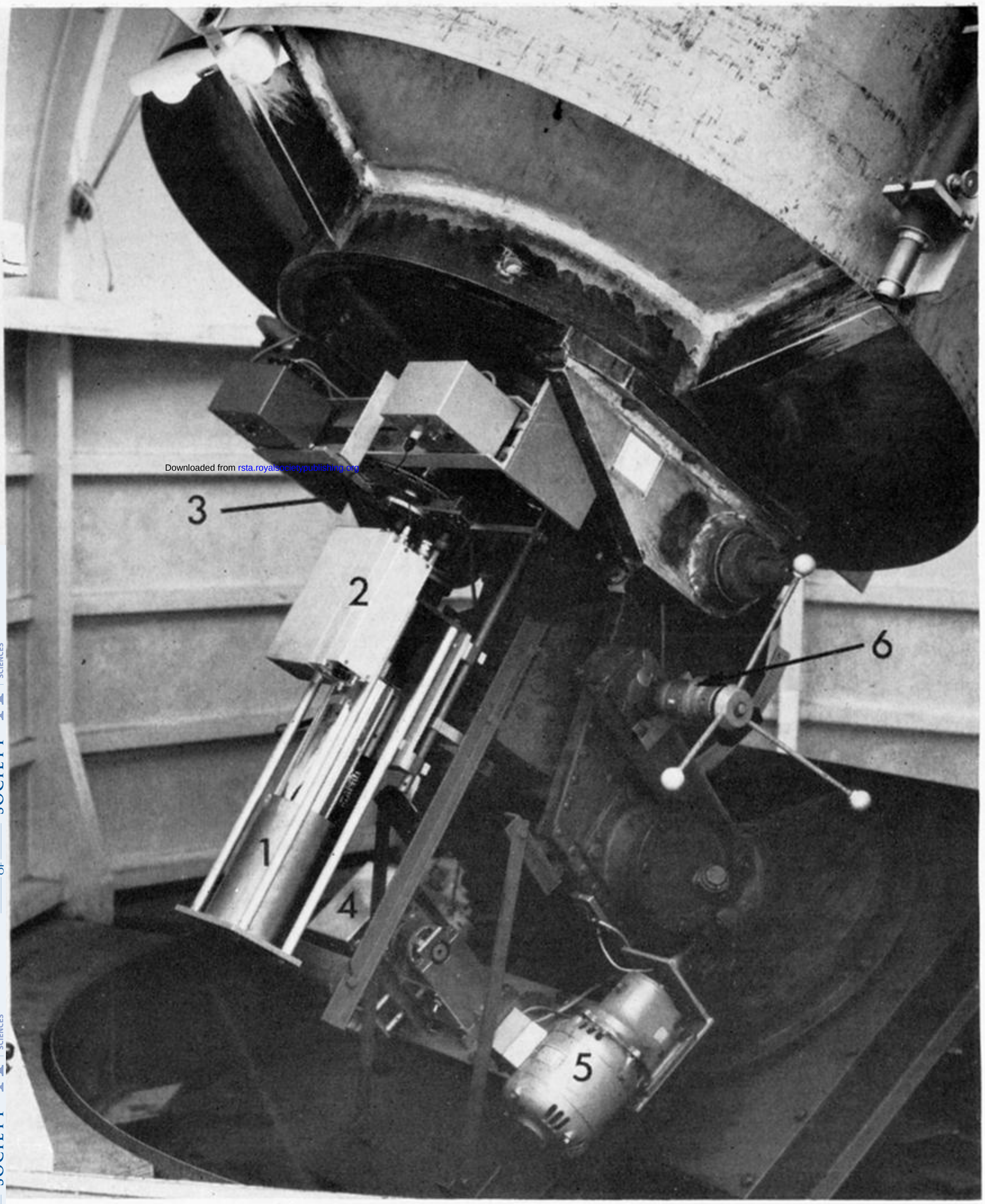

FIGURE 11. Detector mounted on telescope: (1) detector, (2) pre-amplifier and amplifier, (3) chopper, (4) hour angle drive motor; (5) declination drive motor, (6) cams for automatic control.

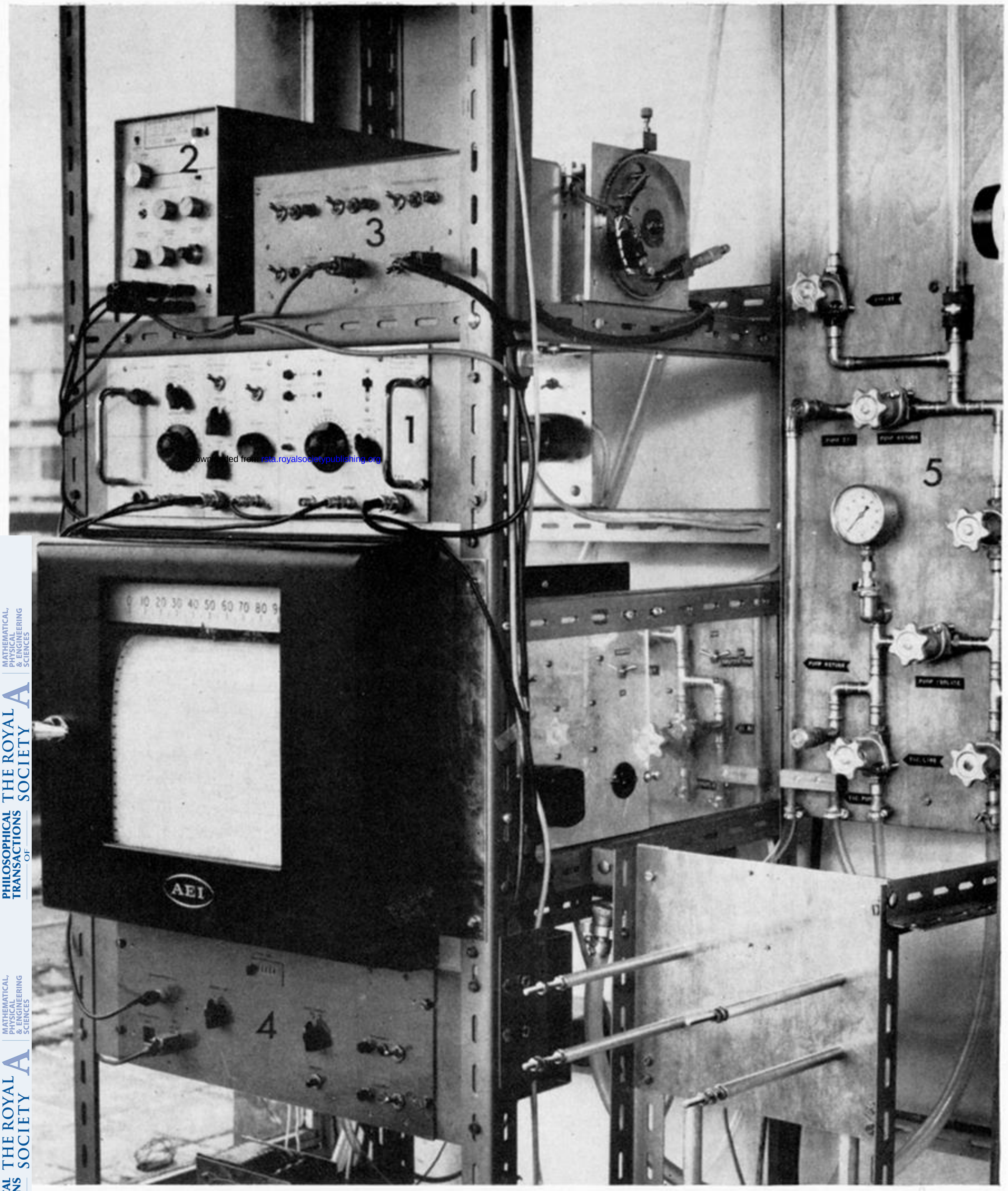

PHILOSOPHICAL TRANSACTIONS OF THE ROYAL SOCIETY A MATHEMATICAL, PHYSICAL & ENGINEERING SCIENCES

FIGURE 12. Automation and data processing equipment: (1) data control panel, (2) Nuclear Data Inc. 'Enhancetron', (3) automation control unit, (4) Enhancetron-triggering and scan-counting unit, (5) helium-transfer system.